Petroleum Science 21 (2024) 2475–2484

Contents lists available at ScienceDirect

Petroleum Science

journal homepage: www.keaipublishing.com/en/journals/petroleum-science

Original Paper

An efficient data-driven global sensitivity analysis method of shale gas production through convolutional neural network

Liang Xue [a, b], Shuai Xu [a, b], Jie Nie [c], Ji Qin [a, b], Jiang-Xia Han [a, b, *], Yue-Tian Liu [a, b], Qin-Zhuo Liao [a, b]

[a] State Key Laboratory of Petroleum Resources and Engineering, China University of Petroleum (Beijing), Beijing, 102249, China
[b] Department of Oil-Gas Field Development Engineering, College of Petroleum Engineering, China University of Petroleum (Beijing), Beijing, 102249, China
[c] Chuanqing Drilling Engineering Co. Ltd., China National Petroleum Corporation, Chengdu, 610051, Sichuan, China

ARTICLE INFO

Article history:
Received 11 August 2023
Received in revised form
6 February 2024
Accepted 21 February 2024
Available online 22 February 2024

Edited by Yan-Hua Sun

Keywords:
Shale gas
Global sensitivity
Convolutional neural network
Data-driven

ABSTRACT

The shale gas development process is complex in terms of its flow mechanisms and the accuracy of the production forecasting is influenced by geological parameters and engineering parameters. Therefore, to quantitatively evaluate the relative importance of model parameters on the production forecasting performance, sensitivity analysis of parameters is required. The parameters are ranked according to the sensitivity coefficients for the subsequent optimization scheme design. A data-driven global sensitivity analysis (GSA) method using convolutional neural networks (CNN) is proposed to identify the influencing parameters in shale gas production. The CNN is trained on a large dataset, validated against numerical simulations, and utilized as a surrogate model for efficient sensitivity analysis. Our approach integrates CNN with the Sobol' global sensitivity analysis method, presenting three key scenarios for sensitivity analysis: analysis of the production stage as a whole, analysis by fixed time intervals, and analysis by declining rate. The findings underscore the predominant influence of reservoir thickness and well length on shale gas production. Furthermore, the temporal sensitivity analysis reveals the dynamic shifts in parameter importance across the distinct production stages.

1. Introduction

As one of the unconventional natural gas resources, the shale gas development has gained dramatic amount of attentions worldwide (Middleton et al., 2017; Shu et al., 2019; Wang and Li, 2017). The shale gas is originated from the organic-rich mudstone or shale that is used to be considered as a source rock not a reservoir rock for oil and gas. The pore throat of the shale matrix is at the micro-scale or even nano-scale with complex structures (Li W. et al., 2016; Mustafa et al., 2021), and the permeability is extremely small with the order of nano-Darcy (Liehui et al., 2019). It is not economically feasible to produce shale gas in its natural conditions. Due to the advancement of horizontal well drilling and hydraulic fracturing techniques, they create the pathway for the shale gas flow from the matrix to the wellbore by increasing the permeability of the stimulation zones (King, 2011). The extended natural fractures and induced hydraulic fractures form the intricate fracture network in the shale matrix (Wang et al., 2009). The storage form of shale gas can be free gas in the void space in the matrix pores and fracture, adsorbed gas on the walls of the pores, and dissolved gas in the kerogen (Javadpour et al., 2010). Because of the multi-scale porous media and the distinctive storage mechanisms, the flow mechanisms of the shale gas are complex (Yu et al., 2016), and the amount of influencing factors of the shale gas production is much larger than that of conventional gas reservoirs. Therefore, it is necessary to develop a method to efficiently identify the dominant influencing parameters.

There are two fundamental ways to create the mapping from shale reservoir parameters and shale gas production. One is the physics-driven model that is targeted to find the hidden flow rules behind the shale gas production. The analytical, semi-analytical method, meshfree method, and edge-based green element method can be used to simulate the shale gas production process. These solutions provide the basis for pressure transient analysis

* Corresponding author. State Key Laboratory of Petroleum Resources and Engineering, China University of Petroleum (Beijing), Beijing, 102249, China.
E-mail address: hanj459@163.com (J.-X. Han).

https://doi.org/10.1016/j.petsci.2024.02.010

(PTA) or rate-transient analysis (RTA) for shale gas production for fractured horizontal well (Ajayi et al., 2011; Cinco-Ley and Samaniego-V., 2007; Gringarten et al., 2007; Gringarten and Ramey, 1973; Guppy et al., 2007). Chen et al. (2018) considered the hydraulic fracture conductivity, cluster spacing, and the permeability of stimulated zone and performed a pressure-transient analysis in the shale gas reservoir developed through a hydraulic fractured horizontal well. The complex fracture geometry in the shale gas reservoir is necessary to be accounted for in the shale gas production solution. Yang et al. (2016) developed a shale gas model to consider real gas transport and complex non-planar fracture networks, and the rate transient behavior is systematically analyzed. Yu et al. (2017) developed a semi-analytical solution for shale gas reservoirs by dividing fractures into small segments to account for the complex non-planar fracture geometry. However, it is challenging to use these analytical methods to capture the characteristics of the reservoir heterogeneity, multiphase gas and water flow, and fracture geometry with arbitrary orientation. The shale gas numerical simulation method can be more flexible to incorporate these fracture and flow characteristics. Rubin (2010) used the local grid refinement method with the structured grid to model the hydraulic fractured reservoir. To increase the accuracy and efficiency of the simulation, small grid cells are placed on the fractures and the grid spacing is logarithmically spaced in the stimulated reservoir volume. Due to the limitation of the grid structures, the local refinement method can only simulate the shale gas reservoir with orthogonal bi-wing fractures. To represent the complex fracture geometry in the real fractured condition, the discrete fracture models are used to simulate the shale gas production with unstructured gridding (Karimi-Fard et al., 2007). Wang and Shahvali (2015) used discrete fracture modeling to simulate the shale gas production with non-linear flow mechanisms, and the centroidal voronoi tessellation (CVT) is developed to characterize the transient flow behavior near hydraulic fractured well. Even though the unstructured gridding method greatly advances the characterization of the complicated fracture distribution, its implementation is associated with an expensive computational cost. Moinfar et al. (2013) developed the embedded discrete fracture model (EDFM) to improve the efficiency. This method can embed the fracture planes directly into the structured grid system, thus it can avoid the complicated unstructured gridding of the shale reservoir and account for the real geometry of the hydraulic fractures. The EDFM simulation method can be integrated with the existing commercial software in a non-intrusive way. Due to the flexibility of the EDFM method to deal with the fracture geometry, it has been used widely in the simulation of unconventional oil and gas reservoirs. Dai et al. (2019) used an unstructured quadrangular grid-based EDFM method to simulate gas production in an irregularly shaped naturally fracture shale reservoir. Xue et al. (2020) used the EDFM-based particle filter method to perform automatic history matching of shale gas reservoirs. Kim et al. (2021) developed a parameterization method for EDFM so that the calibration efficiency can be improved.

With the development of the artificial intelligence algorithm, the data-driven model that uses the observed data to obtain the mapping between model parameters and shale gas production has gained increasing attention (Xue et al., 2023a, 2023b). Lee et al. (2019) used the long short-term-memory method to predict the time-series shale gas production data. Vikara et al. (2020) used the gradient-boosted regression tree (GBRT) method to estimate the oil and gas productivity of the Marcellus shale and optimize the design of the production well. Xue et al. (2023a, 2023b) developed a deep learning model driven jointly by the decline curve analysis model and production data for the production performance prediction of gas wells. Huang et al. (2023) use graph neural networks (GNN) for production forecasting to identify the relationships between injector-producer pairs and producer-producer pairs. The traditional progression of data-driven neural networks has predominantly concentrated on acquiring knowledge of mappings within finite-dimensional Euclidean spaces. In more recent times, this approach has been broadened to encompass neural operators, which specialize in learning mappings across function spaces. In the context of partial differential equations (PDEs), neural operators are designed to adeptly learn the mapping from any functional parametric correlation to the corresponding solution. Consequently, they acquire proficiency in handling an entire spectrum of PDEs, diverging from classical methods that are tailored to solving specific instances of the equation. Wen et al. (2022) introduced U–FNO, an optimized Fourier neural operator, demonstrating its remarkable precision in addressing multiphase flow challenges, especially in the context of CO_2 geological storage. Yan et al. (2022) developed a deep learning workflow based on Fourier neural operators (FNO) to predict the pressure evolution of fluid flow in large-scale 3D heterogeneous geological CO_2 storage reservoirs. To embody the physical consistency of deep learning, Raissi et al. (2019) introduced the physics-informed neural network (PINN) and employed the residuals of nonlinear partial differential equations to guide the training process using automatic differentiation. They extended this approach to address both forward and inverse problems. Wang et al. (2022) proposed a theory-guided convolutional neural network (TgCNN) framework as a surrogate for subsurface flows with position-varying sink/source terms (well locations), which is further utilized for well placement optimization.

The flow mechanisms of shale gas are complex to be characterized and many factors can influence the production performance of the shale gas. It is crucial to identify the influencing factors of the shale gas production. Sensitivity analysis can be used to evaluate the relative importance of the model parameters to the model productions quantitatively. In general, sensitivity analysis can be divided into categories, and they are local and global sensitivity analysis. The local sensitivity analysis method is used to assess the local influence of the input parameters on the model response. It is usually evaluated by using gradients of the output to a given input parameter while keeping the rest of the input parameters fixed. Yu et al. (2014) performed a local sensitivity analysis of fracture geometry on the shale gas production by varying the half-length of the hydraulic fractures. Deng et al. (2015) conducted the local sensitivity analysis of the size of the stimulated reservoir volume (SRV) region, property of the SRV region, fracture number, fracture intervals, dimensionless fracture conductivity coefficient, interporosity flow coefficient, storativity ratio and adsorption coefficient on type curves of pressure transient in shale gas reservoir. The global sensitivity is used to explore the influencing level of all the input parameters on the model response within all the reasonable parameter ranges. The global sensitivity analysis is often conducted through Monte Carlo simulation, and the computational efficiency is low. Therefore, many researches have focused on the improvement of global sensitivity analysis efficiency. Dai et al. (2014) developed the polynomial chaos expansions method to express the reservoir simulation response and used the probabilistic collocation method to obtain the global sensitivity analysis results efficiently. Luo et al. (2018) propose a correlation-based adaptive localization scheme that does not rely on the physical locations of the observations. Rezaei et al. (2020) developed a reduced-order model (ROM) to improve the global analysis efficiency by replacing the fully coupled poroelastic hydraulic fracture model with a computationally efficient analytical model, and it found that the mobility, production pressure, and fracture half-length are the dominant factors.

In contrast to conventional methodologies, this study proposes an innovative data-driven global sensitivity analysis (GSA) technique employing a convolutional neural network (CNN) within the deep learning framework to discern the pivotal parameters influencing shale gas production, as shown in Fig. 1. The CNN, having assimilated intricate data relationships, adeptly captures the input-output mapping crucial for subsequent sensitivity assessments. Additionally, the investigation introduces three distinctive scenarios for sensitivity analysis: an analysis of the production stage in its entirety, an analysis conducted at fixed time intervals during the production stage, and an analysis considering the production stage through the lens of declining rates. This comprehensive methodology facilitates a nuanced comprehension of parameter sensitivities at various stages of shale gas production.

The rest of the paper is organized as follows. In Section 2, the theoretical basis of the GSA and CNN are introduced. In Section 3, the performance of CNN is validated against the embedded discrete modeling method in shale gas production, and the CNN-based GAS results are presented. Finally, the conclusions are drawn in the Section 4.

2. Methodology

2.1. Global sensitivity analysis

The Sobol' method is a variance-based global sensitivity analysis technique employed within a probabilistic framework (Sobol', 2001). Its objective is to partition the variance of a model's or system's output into fractions that can be attributed to individual input parameters or sets of parameters. In the context of the Sobol' sensitivity analysis method, these fractions, whether originating from a single parameter or the interaction of multiple parameters, are expressed as sensitivity indices (SI's) referred to as "Sobol' indices". These indices represent the proportion of the total output variance and can be utilized for both fixed-function (FF) and fixed-point (FP) models. The appeal of variance-based sensitivity measures lies in their capacity to assess sensitivity across the entire input space, making them a global method. Moreover, they are well-suited for capturing sensitivity in nonlinear systems and quantifying the impact of interactions in non-additive systems.

Suppose that $f(\cdot)$ is a square-integrable function defined in the unit hypercube $[0,1]^n$, the output y can be expressed as

$$y = f(\mathbf{x}), \tag{1}$$

where $\mathbf{x}$ is the model input vector defined on an n-dimensional unit hypercube:

$$K^n = \{\mathbf{x} : 0 \leqslant x_i \leqslant 1, i = 1, \ldots, n\}. \tag{2}$$

The function can be written as the summation of a set of elementary functions with increasing dimensions by using Sobol' decomposition (Sobol', 2001):

$$f(x_1, \ldots, x_n) = f_0 + \sum_{i=1}^{n} f_i(x_i) + \sum_{1 \leqslant i < j \leqslant n} f_{ij}(x_i, x_j) + \cdots + f_{1,2,\ldots,n}(x_1, \ldots, x_n), \tag{3}$$

where f_0 is the constant. It is the mean value of the function, and can be expressed as

$$f_0 = \int_{K^n} f(\mathbf{x}) \mathrm{d}\mathbf{x}. \tag{4}$$

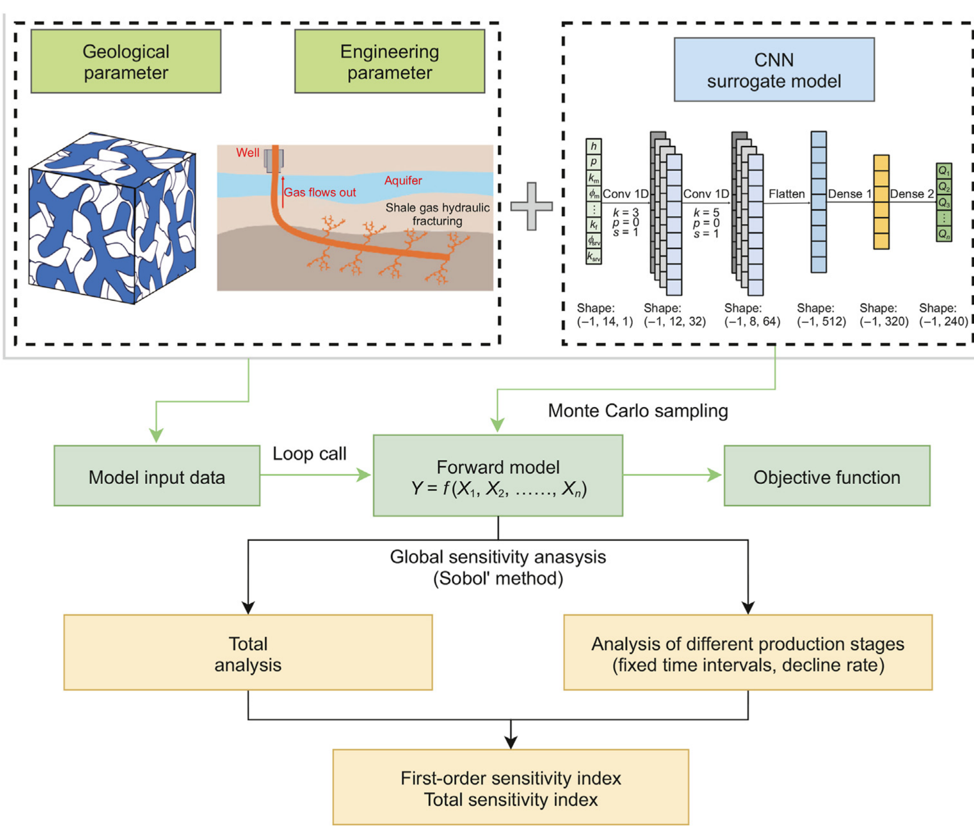

Fig. 1. The main structure of this study.

The univariate terms in the decomposed function can be expressed as

$$f_i(x_i) = \int_{K^{n-1}} f(\mathbf{x})\mathrm{d}\mathbf{x}_{\sim i} - f_0, \tag{5}$$

where the symbol "∼" means the "complementary of".

The total variance of the output function is

$$D = \mathrm{Var}[f(\mathbf{x})] = \int_{K^n} f^2(\mathbf{x})\mathrm{d}\mathbf{x} - f_0^2. \tag{6}$$

By integrating the square of $f(x)$ function and using the orthogonal property, the total variance can be decomposed by

$$D = \sum_{i=1}^{n} D_i + \sum_{1\leqslant i<j\leqslant n} D_{ij} + \cdots + D_{1,2,\ldots,n}, \tag{7}$$

where the partial variances in the summation can be written as

$$D_{i_1,\ldots,i_s} = \int_{K^s} f^2_{i_1,\ldots,i_s}(x_{i_1},\ldots,x_{i_s})\mathrm{d}x_{i_1},\ldots,\mathrm{d}x_{i_s}. \tag{8}$$

The Sobol' indices can be defined as the ratio of the partial variances to the total variance as

$$S_{i_1,\ldots,i_s} = D_{i_1,\ldots,i_s}/D. \tag{9}$$

The Sobol' index can work as a sensitivity measure to describe how much total variance has been accounted for by the uncertainties in the input parameters. The higher Sobol' indice values mean the greater influences on the variation of the output. The influence of the input variables can be ranked according to the magnitude of the Sobol' index.

In practice, the Sobol' indices are computed through Monte Carlo simulation. However, the computational cost to numerically evaluate the integrals in the Sobol' I ndices is very high, especially when the $\boldsymbol{f}(\cdot)$ can not be efficiently solved. Much research has been devoted to improving the computational efficiency of global sensitivity.

2.2. Convolutional neural network

The convolutional neural network (CNN) is a deep learning method designed to perform the image processing (LeCun et al., 2008). It is derived from the traditional ordinary neural network, which is made up of neurons with weights and biases as characterization parameters. CNN can extract the important features automatically from the grid-like arrangement data, such as images, by reducing the computational complexity of setting up the learning model.

There are three types of layers in the CNN architecture: the convolutional layers, pooling layers, and fully-connected layers. The convolutional layer is used to connect to a small local region of the input through a scalar product between the weights and input values. The small region of input connected by the convolutional layer is referred to as the receptive field. Only the input values within the receptive field can affect the extracted features of the convolutional neural network. The weights form a learnable convolutional kernel, which is defined to convolve across the spatial dimensionality of the input to generate a feature map. All the spatial locations share the same convolutional kernel, which greatly reduces the number of parameters required by the convolutional layer. This technique is called "weight sharing" (Nowlan and Hinton, 2018). The convolution kernel is overlapped on top of the input matrix, the product can be computed between the numbers at the same location in the kernel and the input, and a single number can be obtained by summing these products together. By learning the kernel, a specific feature at a given spatial position of the input will be highlighted. Many kernels can be used to extract the feature maps from different perspectives. All the generated feature maps are stacked along the depth dimension to form the fill output from the convolutional layer.

Suppose that the input tensor for a specific convolutional layer is

$$x \in R^{M_1\times M_2}, \tag{10}$$

where M_1 and M_2 are the dimensions of the input; and $x_{i,j}$ is the input value at the position (i,j).

The convolutional kernel is denoted as

$$\omega \in R^{k_1\times k_2}, \tag{11}$$

where k_1 and k_2 are the dimensions of the input; $w(c,d)$ indicates the weight value at the position (c,d) in the convolutional neural network. The variable $u_{i,j}$ is the value of the feature map, and it can be expressed as

$$u_{i,j} = \sum_{c=1}^{k_1}\sum_{d=1}^{k_2} x_{i\cdot s_1-1+c,j\cdot s_2-1+d}\cdot w_{c,d} + b. \tag{12}$$

After passing through the convolutional and pooling layers, the values in a feature map are redefined to a vector and used for the interpretation of the features.

$$u_j = \sum_{i=1}^{n} x_i \cdot w_{i,j} + b_j, \tag{13}$$

where x_i is the input vector; $w_{i,j}$ is the weight; and b_j is the bias.

The learning process is performed using the error back-propagation method, which uses the gradient descent to update the weights. The training process consists of minimizing the cost function by adjusting the weights according to the following equation

$$w_i^{t+1} = w_i^t - \eta\frac{\partial C}{\partial w_i^t}, \tag{14}$$

where w_i^t is the i weight of the network at the current time t; η is the learning rate; and C is the mean-squared loss between the true data and predicted data. In order to avoid this overfitting in its learning, we use the dropout technique. It consists in withdrawing randomly some units from the neural network (Srivastava et al., 2014). In this work, the CNN provides a forward prediction model of the input parameters to the output values of the shale gas production capability through its powerful nonlinear fitting capability trained on a large amount of data, and also serves as a surrogate model for the subsequent sensitivity analysis.

3. Results and discussion

3.1. Construction of CNN-based shale gas production model

The establishment of the dataset utilized for training the data-driven model plays a pivotal role in the realm of deep learning. A copious volume of data characterized by high quality enhances the model's learning efficacy and augments its generalization capabilities on test datasets that remain uninvolved in the model training process. However, practical constraints arise in the context of oilfield production and development. The availability of oilfield blocks and the number of wells drillable within a specific block are inherently limited. Consequently, obtaining an extensive dataset for the training phase, encompassing fracturing and production data, becomes impractical. To address this limitation for theoretical validation, this study employs reservoir numerical simulation software to generate shale gas production processes, thereby establishing a comprehensive dataset for training the convolutional neural network.

Based on the geological properties and engineering parameters of shale gas reservoirs, a numerical model of fracturing horizontal wells in shale gas reservoirs is established through reservoir simulation software, as shown in Fig. 2. A fracturing horizontal well is set up in the model, distributed in the middle region of the targeted area. The hydraulic fractures are explicitly characterized by the embedded discrete fracture model (EDFM) method, and the constant pressure working schedule is adopted. The shale gas is produced with constant bottom-hole pressure for 20 years. The specific value ranges are shown in Table 1.

The model reservoir is assumed to be homogeneous, featuring isotropic permeability. Employing an embedded discrete fracture model, artificial fractures are simulated, with all fractures evenly distributed and positioned perpendicular to the horizontal well section. The SRV area is configured to be incompletely connected, signifying that each hydraulic fracture is associated with a connected rectangular stimulation area; however, these individual rectangular stimulation areas are not interconnected. By selecting different combinations of characteristic parameters within their corresponding ranges, a multitude of geological models can be derived from the foundational geological model. Subsequently, through numerical simulation, various sets of shale gas production characteristics corresponding to these geological models can be obtained. To address potential issues stemming from random sampling, such as the occurrence of repeated parameter combinations or incomplete coverage of certain value ranges, this study employs Latin hypercube sampling to procure 5000 distinct sets of parameter combinations. Subsequently, the dataset is partitioned into a training set, validation set, and test set, comprising 4000, 500, and 500 instances, respectively.

The convolutional neural network (CNN) processes input data consisting of 14 feature parameters. The convolutional layer is configured to extract key features, while the pooling layer reduces the size of the extracted feature data. Subsequently, the flattened layer reshapes the data into a 1-D array, and the fully connected layer makes predictions for the output. The network's structural configuration often requires hyperparameter optimization to achieve optimal predictive performance. This involves fine-tuning parameters, including the number of convolutional layers, the size of convolutional kernels, the number of neurons in fully connected layers, and the batch size. Fig. 3 illustrates the relative errors associated with each parameter on the test set. Consequently, the optimal configuration comprises two convolutional layers, with the first layer featuring a kernel size of 3 and the second layer a kernel size of 5. The fully connected layer is configured with 320 neurons, and the batch size is set at 32. The final model is depicted in Fig. 4.

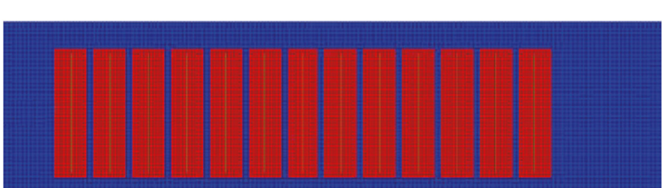

Fig. 2. The geological model of the shale gas reservoir.

Table 1
Basic numerical model parameters.

Key words	Parameter	Minimum	Maximum	Unit
Thick	Reservoir thickness	3	11	m
Init-pre	Initial pressure	350	550	bar
Init-s-w	Initial water saturation	0.15	0.35	/
Mat-perm	Matrix permeability	10^{-5}	10^{-3}	mD
Mat-poro	Matrix porosity	0.02	0.08	/
Lang-v	Langmuir volume	5	15	m^3/m^3
Lang-p	Langmuir pressure	50	100	bar
Srv-perm	SRV permeability	10^{-3}	0.1	mD
Srv-poro	SRV porosity	0.1	0.16	/
Fra-h-len	Fracture half length	150	250	m
Fra-con	Fracture conductivity	0.2	2	mD m
Frac-num	Fracture number	10	100	/
Well- len	Horizontal wellbore length	1000	2000	m
BHP	Bottom hole pressure	10	100	bar

Furthermore, to quantitatively evaluate the test results, the following two metrics are introduced. One is the relative error:

$$r = \frac{\left| y_{\mathrm{t}} - y_{\mathrm{p}} \right|}{y_t}, \tag{15}$$

where the y_{t} is reference value solved by the reservoir simulator and the y_{p} is predictions of CNN, respectively. This formula determines the relative error between the actual value of the data set and the predicted value of the model. In order to measure the relative error of the entire test set, the average relative error of all samples in the test set

$$m_{\mathrm{t}} = \frac{1}{N} \sum_{i}^{N} r_i, \tag{16}$$

where N is the sample size of the test set; and m_{t} represents the relative error of the ith sample on the test set.

3.2. Evaluation of the CNN-based shale gas production

Fig. 5 illustrates the relative error of the test for the 125th, 185th, and 196th samples, showcasing the alignment between predicted production curves and actual production data obtained from numerical simulations. These instances, selected from the 500 test cases, serve as representative examples. The relative error changes depicted in Fig. 5(a) reveal that CNN's predicted results align well with the stable production stage but exhibit deviations during the production declining stage. Conversely, Fig. 5(b) indicates an opposing trend, with CNN effectively capturing the declining stage but experiencing an increase in relative error during the stable production stage. Analyzing the relative error statistical distribution of the 500 samples on the test set based on Fig. 5(e), it is observed that 99.6% of the samples exhibit a prediction error of less than 20%, 88.4% of the samples have a prediction error of less than 10%, and more than half of the samples display a prediction error of less than 5%. These results affirm the exceptional predictive capability of CNN in modeling production dynamics.

The investigation into the sensitivity of production to formation parameters, fracturing parameters, and well parameters encompasses two tasks. Firstly, to validate the accuracy of the convolutional neural network surrogate model, the distribution of sensitivity coefficients for each parameter is compared using two distinct production prediction methods: numerical simulation and convolutional neural network. Secondly, the sensitivity coefficients of the parameters are determined, and a ranking is established based on the total sensitivity coefficients. This enables a

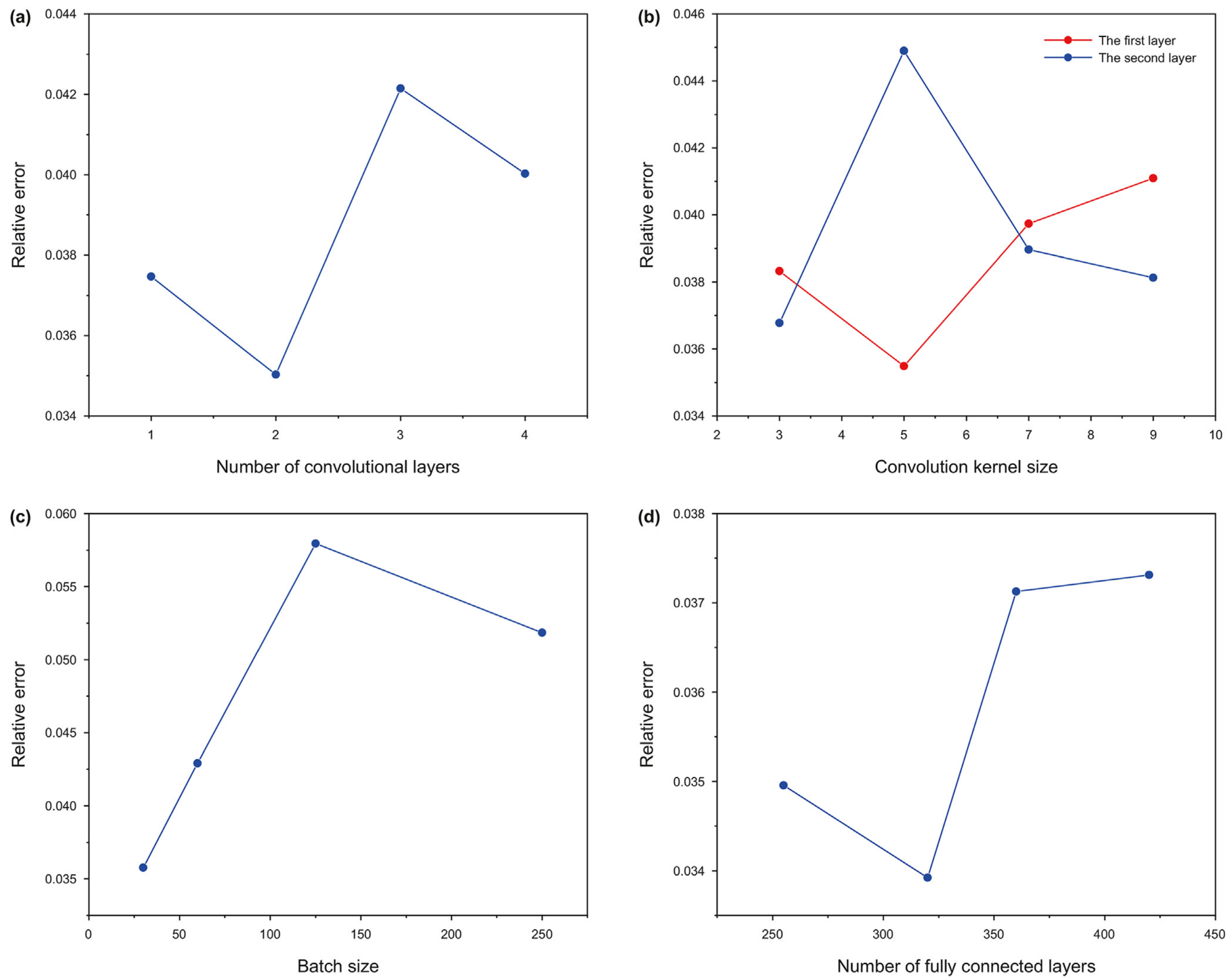

Fig. 3. The hyperparameter optimization of the CNN model.

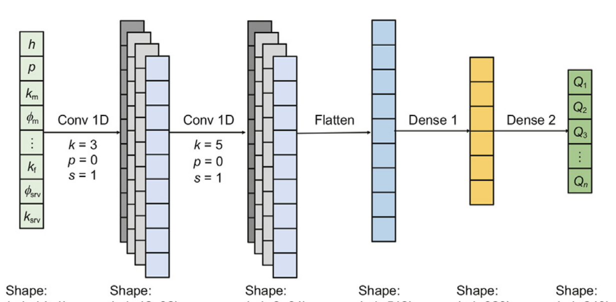

Fig. 4. The final structure of the CNN model.

comprehensive comparison and analysis of the sensitivity of shale gas production to various parameters throughout the entire production period and at different production stages.

3.3. Global sensitivity analysis of shale gas production

When employing the Sobol' method for sensitivity analysis, the Sobol' series is typically utilized to select data samples. However, the Sobol' series encounters the challenge of high repetition in sampling points. To mitigate the error rate in sensitivity coefficient calculations, the sample set is divided using the Saltelli expansion scheme of the Sobol' series. Sensitivity coefficients for 14 parameters are computed based on 20 years of cumulative production, and the parameters are ranked according to their total order sensitivity coefficients, as depicted in Fig. 6. Notably, CNN demonstrates relatively reliable accuracy and sensitivity coefficient trends for the 14 parameters when compared to numerical simulations. Fig. 7 reveals that with a sample set of 5000 and 5 parallel calculation examples, the time consumption for sensitivity analysis using numerical simulation is 80 times greater than that of CNN. Consequently, CNN proves to be a viable surrogate model for numerical simulation, particularly in subsequent sensitivity analysis stages. Among the input parameters, the reservoir thickness and well length exert the most significant influences on shale gas production. This can be attributed to the fact that reservoir thickness determines geological reserves, with larger reserves leading to greater production. Similarly, the well length significantly impacts the hydraulic fractured area, with a larger fractured area resulting in increased production. The initial water saturation, porosity of the SRV area, and the number of fracture segments exhibit moderate effects on production. These parameters influence reserves and the fluid flow capability in the SRV area to some extent. In contrast, the

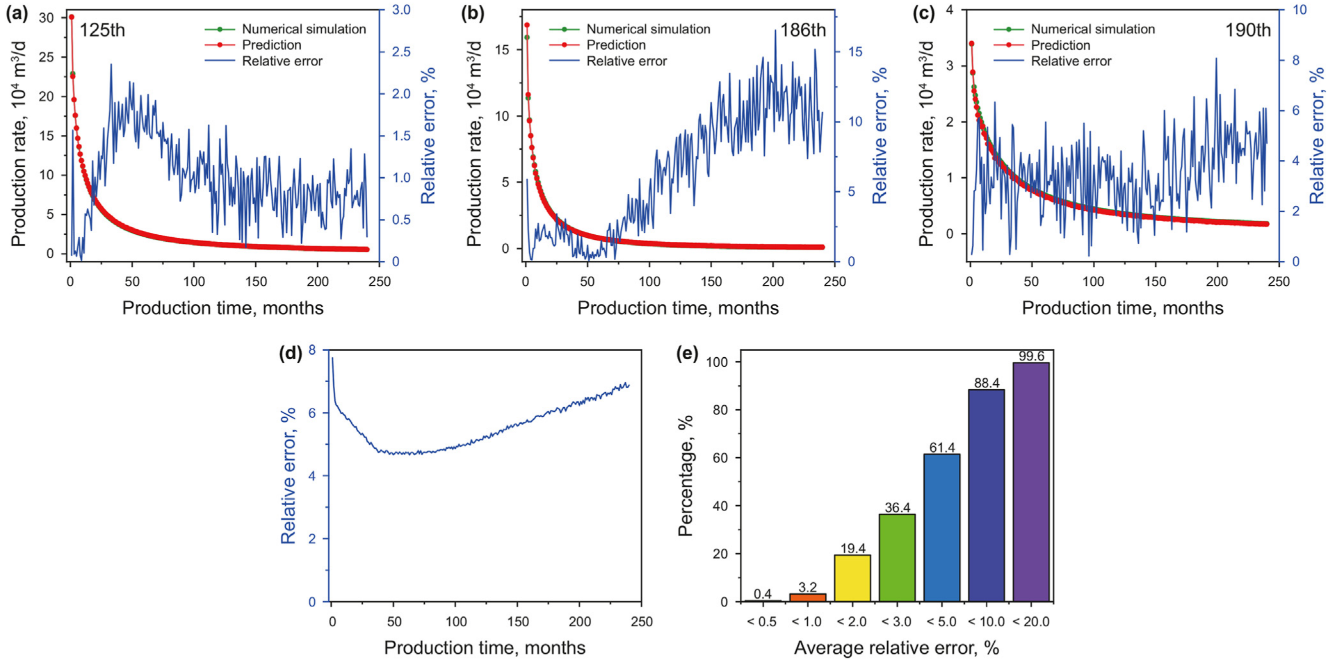

Fig. 5. The CNN model predictions results. (**a**), (**b**), and (**c**) depict predictions for the 125th, 186th, and 190th samples, respectively. The collective performance is summarized in (**d**), representing the average error across all samples. Additionally, (**e**) presents a histogram showcasing the distribution of errors.

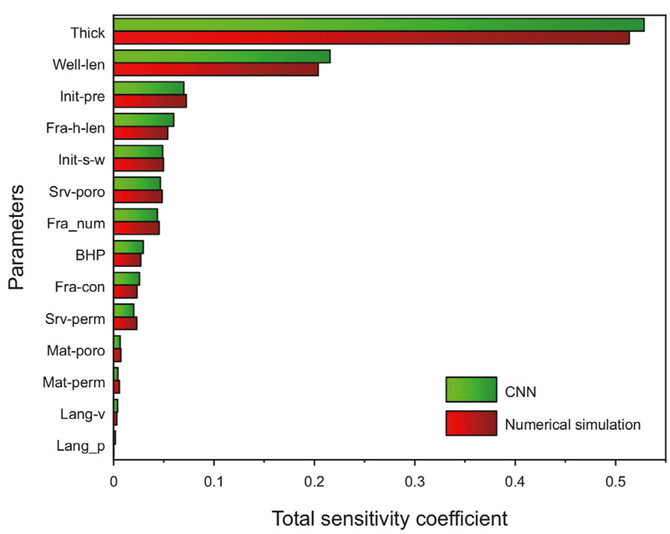

Fig. 6. Comparison of sensitivity coefficients for sensitivity analysis using CNN and numerical simulation.

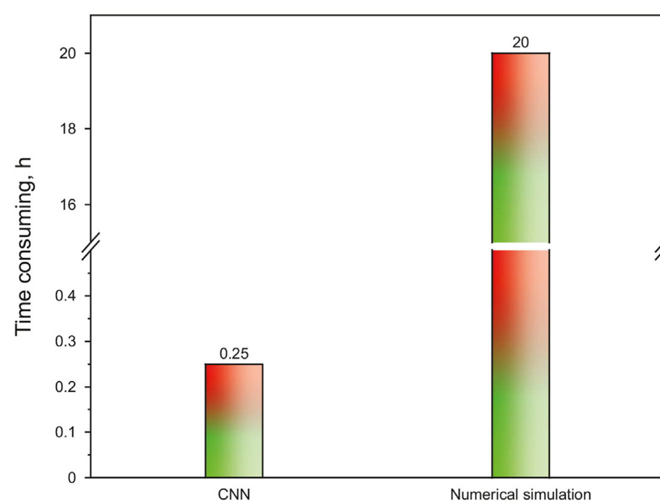

Fig. 7. Time consumed for sensitivity analysis using CNN and numerical simulation for the distribution of 5000 samples.

impact of matrix porosity, permeability, and Langmuir adsorption parameters on production is comparatively weak, with Langmuir pressure being relatively small compared to other parameters. This is attributed to the small contribution of gas production from the peripheral matrix area and the adsorption effect in this scenario, resulting in a less sensitive response to these specific parameters.

3.4. Global sensitivity change at different production stages divided by the fixed time interval

The production stage is segmented into two distinct time intervals: the 0–8 year period, characterized as the declining stage, and the 9–20 year period, denoted as the stable stage. As depicted in Fig. 8, throughout both stages, the predominant sensitive parameters influencing shale gas production remain the reservoir thickness and well length. During the declining stage, production exhibits higher sensitivity to reservoir thickness, initial formation pressure, and initial water saturation. Conversely, in the stable production stage, the sensitivity of parameters such as fracture half-length, bottomhole flow pressure, Langmuir volume, matrix permeability, and porosity becomes notably stronger. The sensitivity coefficients of two-thirds of the parameters exhibit an increase from the declining stage to the stable production stage. Notably, the sensitivity coefficients of reservoir thickness, the number of fracture segments, initial formation pressure, initial water saturation, and porosity of the SRV zone decrease. Among these, the sensitivity of production to initial formation pressure and

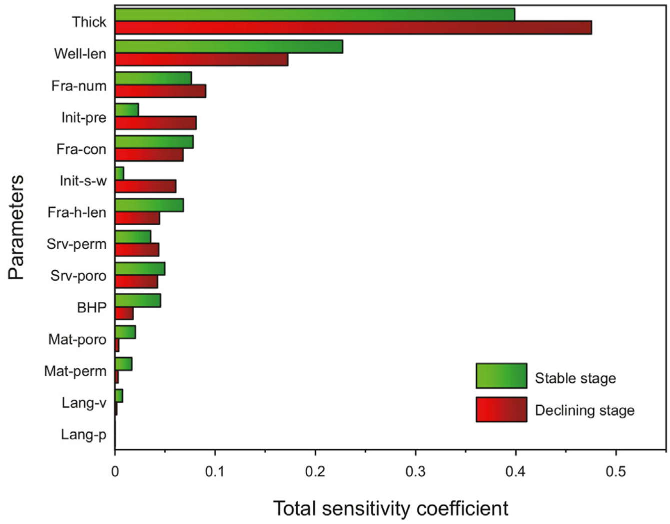

Fig. 8. Comparison of total order sensitivity coefficients for declining and stable production stages based on fixed time interval.

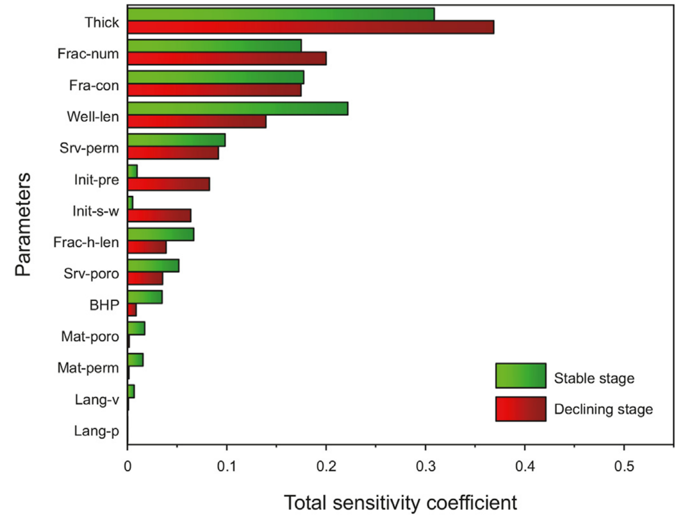

Fig. 9. Comparison of total order sensitivity coefficients for declining and stable production stages based on decline rate.

initial water saturation demonstrates the most significant shift from strong to weak, with sensitivity coefficients reduced by more than 70%, resulting in a one-level decrease in sensitivity ranking. Parameters exhibiting a substantial percentage increase in sensitivity include bottom-hole flow pressure, matrix porosity, matrix permeability, and Langmuir volume, all experiencing an increase of no less than 150%. In the stable production stage, bottom-hole flow pressure not only influences the production pressure difference but also impacts the gas resolution rate, given the proximity of formation pressure to the bottom-hole flow pressure. Additionally, the contribution of the peripheral matrix area and gas adsorption to total production gradually increases, amplifying the influence of the four parameters on production during the stable production stage.

3.5. Global sensitivity change at different production stages divided by the decline rate

The production stage is categorized based on the monthly production decline rate. Specifically, when the decline rate is greater than or equal to 1.5%, it is considered the declining stage; conversely, when the decline rate is less than 1.5%, it is identified as the stable production stage. As illustrated in Fig. 9, the primary sensitive parameters influencing production in both stages remain consistent and include reservoir thickness, the number of fracture segments, fracture conductivity, and well length. During the declining stage, production exhibits higher sensitivity to reservoir thickness, initial formation pressure, and initial water saturation. In contrast, during the stable production stage, the sensitivity of parameters such as fracture half-length, bottom-hole flow pressure, Langmuir volume, matrix permeability, and porosity becomes notably stronger. Similar to the change in parameter sensitivity when divided by fixed production time, 5% of the parameter sensitivity coefficients increased from the declining stage to the stable production stage, where the sensitivity of production to initial formation pressure and initial water saturation changed from strong level to weak level in the most significant way, with an average decrease of 90% in sensitivity coefficients and the sensitivity ranking decreased by one level. The parameters with significantly increased sensitivity include well bottom flow pressure, Langmuir volume, matrix porosity, and permeability, with an increase of no less than 300%.

4. Conclusions

This study presents a pioneering approach to data-driven global sensitivity analysis (GSA) for assessing parameters influencing shale gas production. The innovation lies in the integration of convolutional neural networks (CNN) with the Sobol' method, providing an efficient and robust methodology for sensitivity analysis. The CNN, trained on a comprehensive dataset, serves as a powerful surrogate model, capturing intricate relationships between input parameters and shale gas production. The key contributions of this research can be summarized in three main aspects. Firstly, the coupling of CNN with the Sobol' method offers an efficient means of sensitivity analysis, leveraging CNN's ability to learn complex data relationships. This integration provides a forward prediction model, enabling a thorough exploration of parameter sensitivities. Secondly, the introduction of three distinct sensitivity analysis scenarios adds depth to the framework, allowing for a nuanced understanding of parameter influences at various stages of shale gas production. These scenarios encompass the analysis of the production stage as a whole, analysis by fixed time intervals, and analysis by declining rate. Thirdly, the temporal sensitivity analysis reveals dynamic changes in parameter influence throughout different production stages, shedding light on the varying significance of parameters at different points in time. The findings of the sensitivity analysis highlight the critical role of certain parameters in shale gas production. Across all scenarios, the reservoir thickness and well length consistently emerge as the most influential factors, determining resource reserves and impacting the hydraulic fracture stimulated area. In the analysis of the production stage as a whole, parameters such as initial water saturation, SRV zone porosity, and the number of fracture segments exhibit moderate impacts, influencing resource reserves and fluid flow capacity. Furthermore, the temporal sensitivity analysis underscores the dynamic nature of parameter influences, with reservoir thickness, initial formation pressure, and initial water saturation taking precedence in the declining stage, while parameters like fracture half-length, bottom-hole flow pressure, Langmuir volume, matrix permeability, and porosity become significantly more influential in the stable production stage.

CRediT authorship contribution statement

Liang Xue: Writing – original draft, Conceptualization. **Shuai Xu:** Methodology, Data curation. **Jie Nie:** Data curation, Visualization. **Ji Qin:** Writing – review & editing, Software, Formal analysis, Data curation. **Jiang-Xia Han:** Validation, Supervision, Methodology, Conceptualization. **Yue-Tian Liu:** Data curation, Formal analysis, Methodology. **Qin-Zhuo Liao:** Software, Validation, Visualization.

Declaration of competing interest

The authors declare that they have no known competing financial interests or personal relationships that could have appeared to influence the work reported in this paper.

Acknowledgements

This work was supported by the National Natural Science Foundation of China (Nos. 52274048 and 52374017), Beijing Natural Science Foundation (No. 3222037), and the CNPC 14th five-year perspective fundamental research project (No. 2021DJ2104).

References

Ajayi, B., Walker, K., Wutherich, K., Sink, J., 2011. Channel hydraulic fracturing and its applicability in the marcellus shale. In: SPE East. Reg. Meet. https://doi.org/10.2118/149426-MS.

Chen, Z., Liao, X., Sepehrnoori, K., Yu, W., 2018. A semianalytical model for pressure-transient analysis of fractured wells in unconventional plays with arbitrarily distributed discrete fractures. SPE J. 23, 2041–2059. https://doi.org/10.2118/187290-PA.

Cinco-Ley, H., Samaniego, V.F., 2007. Transient pressure analysis for fractured wells. J. Petrol. Technol. 33, 1749–1766. https://doi.org/10.2118/7490-PA.

Dai, C., Li, H., Zhang, D., 2014. Efficient and accurate global sensitivity analysis for reservoir simulations by use of the probabilistic collocation method. SPE J. 19, 621–635. https://doi.org/10.2118/167609-PA.

Dai, C., Liu, H., Wang, Y., Li, X., Wang, W., 2019. A simulation approach for shale gas development in China with embedded discrete fracture modeling. Mar. Petrol. Geol. 100, 519–529. https://doi.org/10.1016/j.marpetgeo.2018.09.028.

Deng, Q., Nie, R.-S., Jia, Y.-L., Huang, X.-Y., Li, J.-M., Li, H.-K., 2015. A new analytical model for non-uniformly distributed multi-fractured system in shale gas reservoirs. J. Nat. Gas Sci. Eng. 27, 719–737. https://doi.org/10.1016/j.jngse.2015.09.015.

Gringarten, A.C., Ramey, H.J., 1973. The use of source and Green's functions in solving unsteady-flow problems in reservoirs. SPE J. 13, 285–296. https://doi.org/10.2118/3818-PA.

Gringarten, A.C., Ramey, H.J., Raghavan, R., 2007. Unsteady-state pressure distributions created by a well with a single infinite-conductivity vertical fracture. SPE J. 14, 347–360. https://doi.org/10.2118/4051-PA.

Guppy, K.H., Cinco-Ley, H., Ramey, H.J., Samaniego, V.F., 2007. Non-Darcy flow in wells with finite-conductivity vertical fractures. SPE J. 22, 681–698. https://doi.org/10.2118/8281-PA.

Huang, H., Gong, B., Sun, W., 2023. A deep-learning-based graph neural network-long-short-term memory model for reservoir simulation and optimization with varying well controls. SPE J. 1–19. https://doi.org/10.2118/215842-PA.

Javadpour, F., Fisher, D., Unsworth, M., 2010. Nanoscale gas flow in shale gas sediments. J. Can. Petrol. Technol. 46. https://doi.org/10.2118/07-10-06.

Karimi-Fard, M., Durlofsky, L.J., Aziz, K., 2007. An efficient discrete-fracture model applicable for general-purpose reservoir simulators. SPE J. 9, 227–236. https://doi.org/10.2118/88812-PA.

Kim, H., Onishi, T., Chen, H., Datta-Gupta, A., 2021. Parameterization of embedded discrete fracture models (EDFM) for efficient history matching of fractured reservoirs. J. Petrol. Sci. Eng. 204, 108681. https://doi.org/10.1016/j.petrol.2021.108681.

King, G.E., 2011. Thirty years of gas shale fracturing: what have we learned?. In: SPE Ann. Tech. Conf. Exhib https://doi.org/10.2118/133456-MS.

LeCun, Y., Boser, B., Denker, J.S., Henderson, D., Howard, R.E., Hubbard, W., Jackel, L.D., 2008. Backpropagation applied to handwritten zip code recognition. Neural Comput. 1, 541–551. https://doi.org/10.1162/neco.1989.1.4.541.

Lee, K., Lim, J., Yoon, D., Jung, H., 2019. Prediction of shale-gas production at duvernay formation using deep-learning algorithm. SPE J. 24, 2423–2437. https://doi.org/10.2118/195698-PA.

Li, S., Yang, B., Qi, F., 2016. Accelerate global sensitivity analysis using artificial neural network algorithm: case studies for combustion kinetic model. Combust. Flame 168, 53–64. https://doi.org/10.1016/j.combustflame.2016.03.028.

Li, W., Wang, C., Shi, Z., Wei, Y., Zhou, H., Deng, K., 2016. The description of shale reservoir pore structure based on method of moments estimation. PLoS One 11, e0151631. https://doi.org/10.1371/journal.pone.0151631.

Liehui, Z., Baochao, S., Yulong, Z., Zhaoli, G., 2019. Review of micro seepage mechanisms in shale gas reservoirs. Int. J. Heat Mass Tran. 139, 144–179. https://doi.org/10.1016/j.ijheatmasstransfer.2019.04.141.

Luo, X., Bhakta, T., Nævdal, G., 2018. Correlation-based adaptive localization with applications to ensemble-based 4D-seismic history matching. SPE J. 23, 396–427. https://doi.org/10.2118/185936-PA.

Middleton, R.S., Gupta, R., Hyman, J.D., Viswanathan, H.S., 2017. The shale gas revolution: barriers, sustainability, and emerging opportunities. Appl. Energy 199, 88–95. https://doi.org/10.1016/j.apenergy.2017.04.034.

Moinfar, A., Varavei, A., Sepehrnoori, K., Johns, R.T., 2013. Development of an efficient embedded discrete fracture model for 3D compositional reservoir simulation in fractured reservoirs. SPE J. 19, 289–303. https://doi.org/10.2118/154246-PA.

Mustafa, A., Tariq, Z., Mahmoud, M., Radwan, A.E., Abdulraheem, A., Abouelresh, M.O., 2021. Data-driven machine learning approach to predict mineralogy of organic-rich shales: an example from Qusaiba Shale, Rub' al Khali Basin, Saudi Arabia. Mar. Petrol. Geol. 137, 105495. https://doi.org/10.1016/j.marpetgeo.2021.105495.

Nowlan, S.J., Hinton, G.E., 2018. Simplifying neural networks by soft weight sharing. Math. Generaliz. 373–394.

Raissi, M., Perdikaris, P., Karniadakis, G.E., 2019. Physics-informed neural networks: a deep learning framework for solving forward and inverse problems involving nonlinear partial differential equations. J. Comput. Phys. 378, 686–707. https://doi.org/10.1016/j.jcp.2018.10.045.

Rezaei, A., Nakshatrala, K.B., Siddiqui, F., Dindoruk, B., Soliman, M., 2020. A global sensitivity analysis and reduced-order models for hydraulically fractured horizontal wells. Comput. Geosci. 24, 995–1029. https://doi.org/10.1007/s10596-019-09896-7.

Rubin, B., 2010. Accurate simulation of non-Darcy flow in stimulated fractured shale reservoirs. In: SPE Western Reg. Meet. https://doi.org/10.2118/132093-MS.

Shu, Y., Lu, Y., Chen, L., Wang, C., Zhang, B., 2019. Factors influencing shale gas accumulation in the lower Silurian Longmaxi formation between the north and South Jiaoshiba area, Southeast Sichuan Basin, China. Mar. Petrol. Geol. 111, 905–917. https://doi.org/10.1016/j.marpetgeo.2019.06.029.

Sobol, I.M., 2001. Global sensitivity indices for nonlinear mathematical models and their Monte Carlo estimates. Math. Comput. Simulat. 55, 271–280. https://doi.org/10.1016/S0378-4754(00)00270-6.

Srivastava, N., Hinton, G., Krizhevsky, A., Sutskever, I., Salakhutdinov, R., 2014. Dropout: a simple way to prevent neural networks from overfitting. J. Mach. Learn. Res. 15, 1929–1958.

Vikara, D., Remson, D., Khanna, V., 2020. Machine learning-informed ensemble framework for evaluating shale gas production potential: case study in the Marcellus Shale. J. Nat. Gas Sci. Eng. 84, 103679. https://doi.org/10.1016/j.jngse.2020.103679.

Wang, F.P., Reed, R.M., John, A., Katherine, G., 2009. Pore networks and fluid flow in gas shales. In: SPE Ann. Tech. Conf. Exhib. https://doi.org/10.2118/124253-MS.

Wang, N., Chang, H., Zhang, D., Xue, L., Chen, Y., 2022. Efficient well placement optimization based on theory-guided convolutional neural network. J. Petrol. Sci. Eng. 208, 109545. https://doi.org/10.1016/j.petrol.2021.109545.

Wang, Q., Li, R., 2017. Research status of shale gas: a review. Renew. Sustain. Energy Rev. 74, 715–720. https://doi.org/10.1016/j.rser.2017.03.007.

Wang, Y., Shahvali, M., 2015. Discrete fracture modeling using Centroidal Voronoi grid for simulation of shale gas plays with coupled nonlinear physics. Fuel 163, 65–73. https://doi.org/10.1016/j.fuel.2015.09.038.

Wen, G., Li, Z., Azizzadenesheli, K., Anandkumar, A., Benson, S.M., 2022. U-FNO—an enhanced Fourier neural operator-based deep-learning model for multiphase flow. Adv. Water Resour. 163, 104180. https://doi.org/10.1016/j.advwatres.2022.104180.

Xue, L., Liu, Y., Nan, T., Liu, Q., Jiang, X., 2020. An efficient automatic history matching method through the probabilistic collocation based particle filter for shale gas reservoir. J. Petrol. Sci. Eng. 190, 107086. https://doi.org/10.1016/j.petrol.2020.107086.

Xue, L., Li, D., Dou, H., 2023a. Artificial intelligence methods for oil and gas reservoir development: current progresses and perspectives. Adv. Geo-Energy Res. 10 (1), 65–70. https://doi.org/10.46690/ager.2023.10.07.

Xue, L., Wang, J., Han, J., Yang, M., Mwasmwasa, M., Nanguka, F., 2023b. Gas well performance prediction using deep learning jointly driven by decline curve analysis model and production data. Adv. Geo-Energy Res. 3, 15–169. https://doi.org/10.46690/ager.2023.06.03.

Yan, B., Harp, D.R., Chen, B., Pawar, R.J., 2022. Improving deep learning performance for predicting large-scale porous-media flow through feature coarsening. Sci. Rep. 12, 20667. https://doi.org/10.1038/s41598-022-24774-6.

Yang, R., Huang, Z., Yu, W., Li, G., Ren, W., Zuo, L., Tan, X., Sepehrnoori, K., Tian, S., Sheng, M., 2016. A comprehensive model for real gas transport in shale formations with complex non-planar fracture networks. Sci. Rep. 6, 1–13. https://doi.org/10.1038/srep36673.

Yu, W., Luo, Z., Javadpour, F., Varavei, A., Sepehrnoori, K., 2014. Sensitivity analysis of hydraulic fracture geometry in shale gas reservoirs. J. Petrol. Sci. Eng. 113, 1–7. https://doi.org/10.1016/j.petrol.2013.12.005.

Yu, W., Wu, K., Sepehrnoori, K., Xu, W., 2016. A comprehensive model for simulation of gas transport in shale formation with complex hydraulic-fracture geometry. SPE Reservoir Eval. Eng. 20, 547–561. https://doi.org/10.2118/178747-PA.

Yu, W., Xu, Y., Liu, M., Wu, K., Sepehrnoori, K., 2017. Simulation of shale gas transport and production with complex fractures using embedded discrete fracture model. AIChE J. 64, 2251–2264. https://doi.org/10.1002/aic.16060.